crystals

MDPI

Article

A Crystallographic Study on the Growth of Partially Faceted $MnSn_2$ Phase during Solidification Process

Lei Li [1,2,*], Yuantong Bi [1,2], Chunyan Ban [1,2], Haitao Zhang [1,2], Tie Liu [1,2], Xiangjie Wang [1,2], Claude Esling [3,4] and Jianzhong Cui [1,2]

1 Key Laboratory of Electromagnetic Processing of Materials, Ministry of Education, Northeastern University, Shenyang 110819, China; ytong_bi@163.com (Y.B.); bancy@epm.neu.edu.cn (C.B.); haitao_zhang@epm.neu.edu.cn (H.Z.); liutie@epm.neu.edu.cn (T.L.); wangxj@epm.neu.edu.cn (X.W.); jzcui@epm.neu.edu.cn (J.C.)
2 School of Materials Science and Engineering, Northeastern University, Shenyang 110819, China
3 CNRS, Arts et Métiers ParisTech, LEM3, Université de Lorraine, F-57000 Metz, France; claude.esling@univ-lorraine.fr
4 Laboratory of Excellence on Design of Alloy Metals for low-mAss Structures (DAMAS), Université de Lorraine, 57073 Metz, France
* Correspondence: lilei@epm.neu.edu.cn; Tel.: +86-24-8368-7734

Received: 11 September 2018; Accepted: 27 September 2018; Published: 29 September 2018

Abstract: The growth of $MnSn_2$ phase during the solidification process of Sn-Mn alloy was crystallographically investigated. The results show that the non-faced spherical caps of the $MnSn_2$ crystals follow the continuous growth mechanism to grow rapidly along the <001> direction, while the side surfaces the two-dimensional nucleation mechanism to form the low index {100} and {110} facets. An interface structure analysis indicates that the atom planes within the {100} interplanar spacing period (IPSP) has a lower average reticular density than those within the {011} IPSP. This leads to the faster growth rates and thus the shortening and disappearance of the {100} side facets. As a consequence, the partially faceted (i.e., non-faceted spherical caps and faceted side surfaces) $MnSn_2$ crystals follow an octagonal-base/spherical-cap geometric model (few crystals possess square bases) in three dimensions.

Keywords: $MnSn_2$ phase; solidification; crystal growth; crystallography

1. Introduction

$MnSn_2$ crystallizes in a body-centered tetragonal C16 structure ($CuAl_2$-type), consisting of alternating layers of Mn and Sn perpendicular to the crystallographic *c*-axis [1]. Correlated with its structure, $MnSn_2$ exhibited unusual magnetic properties and thereby aroused great interest of researchers in the 1960s [2]. Later in the 1980s, $MnSn_2$ was proposed as an erasable optical recording medium [3]. In recent years, this intermetallic compound was studied more extensively because of its use as electrode materials [4–6]. Despite these investigations, however, little work has been performed on the growth of $MnSn_2$ during solidification process, which is of practical significance considering its increasing use.

It is known that crystal growth is intimately correlated with internal structure. For the tetragonal crystals with the *c*-axis shorter than the *a*-axis, like Al_3Zr (a = 3.998 Å and c = 17.28 Å [7]) [8] and Al_3Ti (a = 3.8537 Å and c = 8.5839 Å [9]) [10], it has been found that they generally grow slowly along the <001> direction and finally exhibit tabular shapes. Based on the atomic arrangement in different crystallographic planes, it was concluded that their growth morphologies are, in a large part, determined by their structures. For the tetragonal crystals with the *c*-axes shorter than the *a*-axes, like

$CuAl_2$ (a = 6.067 Å and c = 4.877 Å [11]) [12] and $CoSn_2$ (a = 6.363 Å and c = 5.456 Å [13]) [14], it has been shown that they usually form an elongated shape due to the preferential growth along the <001> direction. However, there are few studies that connect their growth morphologies with the internal structures. Therefore, it is of fundamental interest to investigate the growth of such type of crystals. The tetragonal $MnSn_2$ crystal just has a shorter c-axis (c = 5.447 Å) than the a-axis (a = 6.659 Å) [13]. A study on its growth may further contribute to the understanding of the relationship between the external morphology and the internal structure of tetragonal crystals.

In view of this background, it was decided to study the growth of $MnSn_2$ phase during the solidification process of Sn-Mn alloy from the point of view of crystallography.

2. Results and Discussion

Figure 1a shows the backscattered electron (BSE) image of the solidified Sn-Mn alloy. The dark gray primary $MnSn_2$ crystals embedded in the light gray β-Sn matrix exhibit bar- or block-like shapes. Figure 1b–e show some typical magnified shapes of the $MnSn_2$ crystals, which have ideal orientations with respect to the observation plane. In Figure 1b, the bar-like crystal has macroscopically smooth interface along the long dimension but rounded ones at tops, showing a partially-faceted growth character. In Figure 1c,d, both crystals possess octagonal shapes, but the former is approximately regular while the latter non-regular. In Figure 1e, a square-shaped crystal can be observed (such square-shaped crystals are rarely spotted in the microstructure). Obviously, all the crystals in Figure 1c–e reveal faceted growth characters.

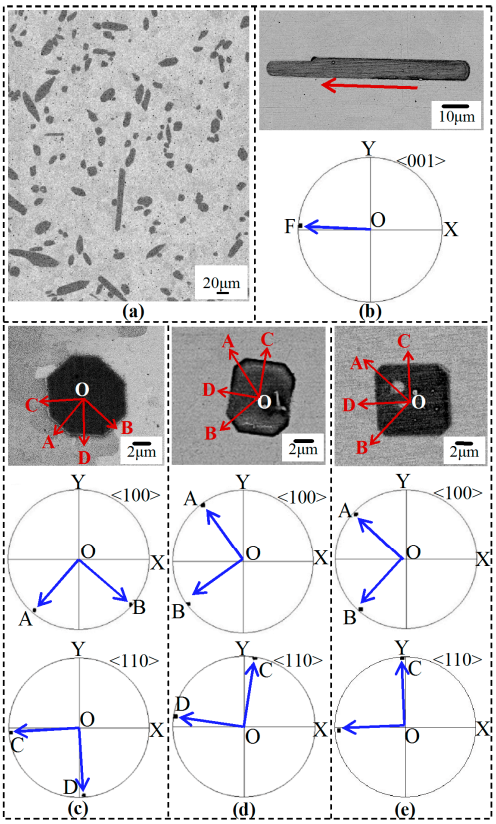

Figure 1. BSE image of (**a**) the solidified Sn-Mn alloy; Typical magnified images of the $MnSn_2$ crystals with (**b**) bar-like, (**c**) approximately regular octagonal, (**d**) non-regular octagonal and (**e**) square shapes, respectively. The <001> pole figure in (**b**) indicates the growth direction of the bar-like crystal (the projection line OF is parallel to the interface trace of the crystal); the <100> and <110> pole figures in (**c**–**e**) illustrate the side facets binding the octagonal and square bases (the projection lines OA, OB, OC and OD are parallel to the normals OA, OB, OC and OD of the side surface traces of the crystals, respectively).

To deeply understand the morphologies of the $MnSn_2$ crystals, a crystallographic analysis was also conducted. In Figure 1b, the projection line OF in the <001> pole figure is parallel to the principal extension direction of the bar-like crystal, indicating a preferential growth along the <001> direction. In Figure 1c–e, the poles A and B in the <100> pole figures are all located near the outermost circles, suggesting that the octagonal and square surfaces are parallel to the {001} plane. Based on this analysis along with the shapes above, it can be deduced that a typical primary $SnMn_2$ crystal should have an elongated prism-like shape in three dimensions. The two-dimensional (2D) octagonal and square shapes just result from the transverse cut of these prism-like crystals by the observation plane. To evidence this, Figure 2a shows a deep-etched SEM image of some $SnMn_2$ crystals. Obviously, they follow an octagonal-base/spherical-cap geometric model, which is totally different from the aforementioned tabular Al_3Ti and Al_3Ti compounds [8,10]. The 3D shapes of truncated octagonal and square bases can be observed in Figure 2b,c, respectively.

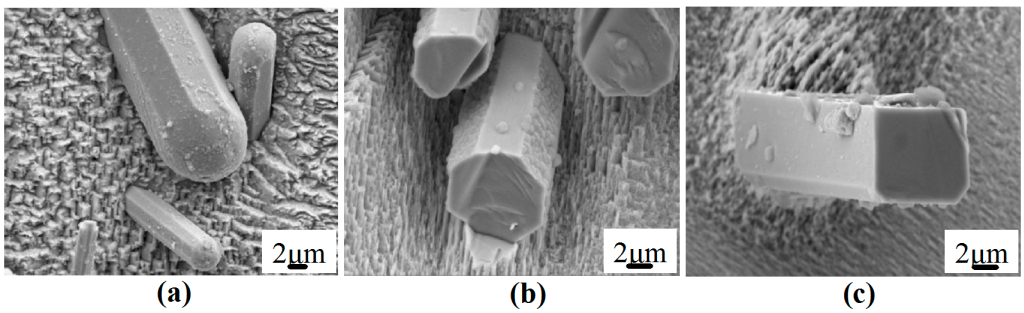

Figure 2. Deep-etched SEM image of (**a**) spherical-capped, (**b**) truncated octagonal-based and (**c**) truncated square-based $MnSn_2$ crystals, respectively.

Since the caps of $MnSn_2$ crystals are spherical (non-faceted), it is difficult to determine a fixed crystallographic plane. However, the side facets can be crystallographically identified. With the indirect two-trace analysis method [15,16], it is determined that the side facets of the octagonal base are from the {100} and {110} families while those of the square base from the {110} family. This result can be further visually demonstrated by the <100> and <110> pole figures in Figure 1c–e (the projection lines OA, OB, OC and OD are parallel to the normals OA, OB, OC and OD of the side surface traces of the $MnSn_2$ crystals, respectively). However, it is worth noting that both the shorter sides in Figure 1d and the vanished sides in Figure 1e correspond to the family of {100} planes.

Crystal growth is a stage following the nucleation, which in a large part determines the final solidification morphology of the crystals. So far, two major crystal growth mechanisms have been well developed [17], i.e., the continuous growth mechanism and the two-dimensional nucleation mechanism. For the former, the solid-liquid interface is ideally diffusive, so most of the lattice sites are favorable for deposition of atoms. Consequently, the interface moves forward uniformly. Such growth mechanism is usually characterized by a relatively rapid growth, and the final morphology of the crystal is smooth in macroscopic scale (non-faceted). For the latter, the interface is assumed to be atomically smooth, so it is not easy for the lattice sites to absorb atoms. In this case, a distribution of surface clusters (suggested as monolayer island nuclei in the Gibbs–Volmer theory [18]) must be formed on the plane surface before the crystal surface can continue to grow. This is because that the clusters (or nuclei) can provide energetically favorable steps for surface adsorbed atoms that become a part of the crystal structure [19]. In such a lateral growth manner, the crystal surface advances continuously. By this growth mechanism, the surface of the final crystal often consists of particular edges and faces (faceted morphology) [17].

In this work, the spherical caps of the $MnSn_2$ crystals should follow the continuous growth mechanism, as a result of which the $MnSn_2$ crystals grow rapidly along the <001> direction and finally form an elongated shape. For the side surfaces of the $MnSn_2$ crystals, the faceted morphology suggests that they should grow by the two-dimensional nucleation mechanism, i.e., clusters (or nuclei) are

firstly formed on the plane surfaces to facilitate the atom absorption. However, it should be noted that the nucleation capabilities on different low index planes vary as their interface structures are different. Figure 3a,b show the 3D atomic structures of the {100} and {110} planes of the $MnSn_2$ phase, respectively. From the Mn atom layers, it seems that the {110} plane is rougher than the {100} plane. To compare the structures of these two planes more quantitatively, a reticular density calculation is helpful. The reticular density ρ is defined as the number of atoms per unit area on a plane [20]. For $\rho_{\{h\,k\,l\}}$, the atoms involved in number counting usually only refer to those having centers that lie on the specific {h k l} plane. However, such density sometimes cannot reflect the underlying interface structure. This is because that there exist additional atom planes instead of only one within an interplanar spacing period (IPSP) in complex crystal structures. Figure 4a shows the $< 00\bar{1} >$ projection view of the $MnSn_2$ structure. As can be observed, there are six ($P^1_{\{100\}}$–$P^6_{\{100\}}$) and four ($P^1_{\{110\}}$–$P^4_{\{110\}}$) planes within the {100} and {110} IPSPs, respectively. Using the new planar density (equivalent to the reticular density ρ) calculating method [21], we get $\rho_{P^1_{\{100\}}} = \rho_{P^2_{\{100\}}} = \rho_{P^6_{\{100\}}} = 0.05528$ atoms/Å^2, $\rho_{P^1_{\{110\}}} = \rho_{P^3_{\{110\}}} = 0.07819$ atoms/Å^2 and $\rho_{P^2_{\{110\}}} = \rho_{P^4_{\{110\}}} = 0.03908$ atoms/Å^2. If we define the average reticular density within the {h k l} IPSP as $\overline{\rho}_{P^{1\text{-}i}_{\{h\,k\,l\}}} = \Sigma\rho_{P^i_{\{h\,k\,l\}}} \cdot S_{P^i_{\{h\,k\,l\}}} / \Sigma S_{P^i_{\{h\,k\,l\}}}$ (S is the area of the $P^i_{\{h\,k\,l\}}$ plane), we obtain $\overline{\rho}_{P^{1\text{-}6}_{\{100\}}} < \overline{\rho}_{P^{1\text{-}4}_{\{110\}}}$ (i.e., 0.05528 atoms/Å^2 < 0.05864 atoms/Å^2).

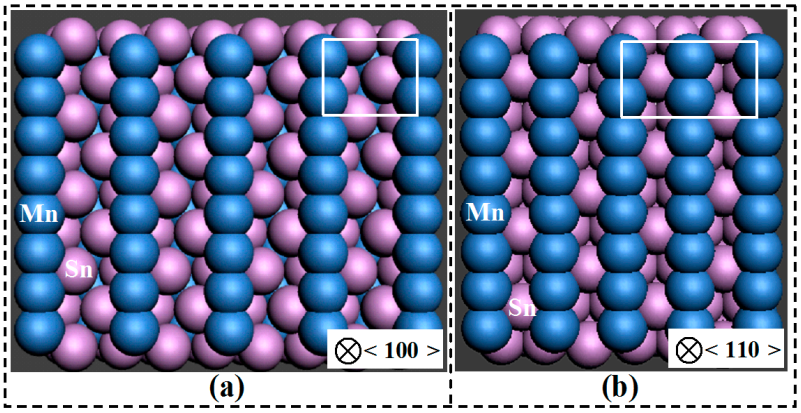

Figure 3. 3D atomic structures of the (**a**) {100} and (**b**) {110} planes of the $MnSn_2$ phase. The rectangular frames enclose a unit cell in (**a**,**b**), respectively.

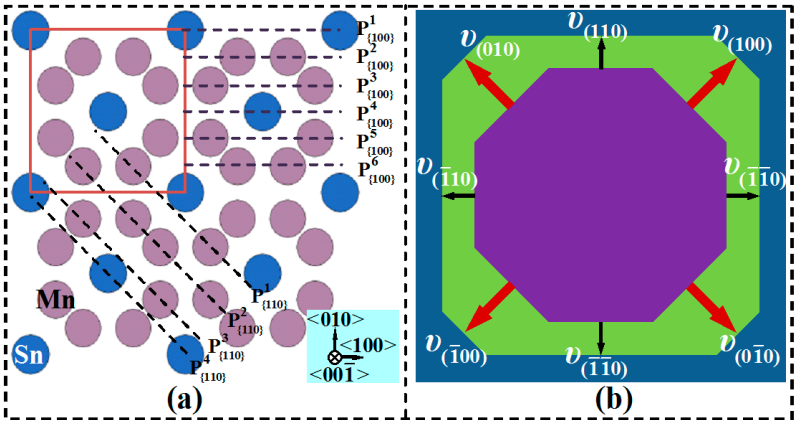

Figure 4. $< 00\bar{1} >$ projection view (**a**) of the $MnSn_2$ structure; schematic diagram (**b**) illustrating the shortening and disappearance of the {100} planes due to their faster growth rate than the {110} planes (the octagonal base tends to develop into a square base). The rectangular frame in (**a**) encloses a unit cell. The dashed lines in (**a**) indicate the ($P^1_{\{100\}}$-$P^6_{\{100\}}$) and ($P^1_{\{110\}}$-$P^4_{\{110\}}$) atom planes within the {100} and {110} interplanar spacing periods, respectively. v with the subscripts referring to the planes in (**b**) indicate the growth rates of the {100} and {110} planes, respectively.

According to the Bravais Law [22], the crystal planes having lower reticular density grow more rapidly than the planes of higher reticular density due to the larger attraction ability to the outside atoms. Thus, the {100} planes of the $MnSn_2$ crystals should have a higher 2D nucleation capability. In other words, the {100} planes can accumulate more critically sized clusters (or nuclei) than the {110} planes to cover the entire surface. As a consequence, the {100} planes have a faster growth rate than the {110} planes. This also explains why the {100} planes tend to get shorter (Figure 1d) and then disappear (Figure 1e), as schematically illustrated in Figure 4b (the octagonal base tends to develop into a square base).

3. Materials and Methods

Sn-1.5 wt.% Mn alloy was prepared with pure metals of Sn (99.95 wt.%) and Mn (99.9 wt.%). A rod was cut from the alloy and then put into a tube of high-purity corundum crucible. The crucible containing the rod was placed in a vacuum resistance furnace and then heated up to 380 °C at a rate of 5 °C/min under argon atmosphere. After being held at this temperature for 20 min, the melt was furnace-cooled to room temperature (the average cooling rate was about 6 °C/min). A specimen was cut lengthwise from the solidified ingot (Φ 10 × 12 mm), following a standard mechanical polishing. The microstructure was observed by a Zeiss ULTRA PLUS FE-SEM (Field-Emission Scanning Electron Microscope, Carl Zeiss, Jena, Germany). After further polishing plus argon ion beam cleaning, individual EBSD (Electron Backscatter Diffraction) orientation measurements of the $MnSn_2$ phase were performed on manually chosen points by the same FE-SEM (equipped with an Oxford-HKL Channel 5 system) as above. To reveal the 3D shape of the $MnSn_2$ phase, a deep etching of the specimen was performed in a solution of 5% NaOH and 3.5% orthonitrophenol in distilled water at 60 °C for 3 min and washed in an ultrasonic ethanol bath.

The side facets binding the $MnSn_2$ phase were determined by an indirect two-trace method [15,16]. By making use of two independent interface trace vectors from one uniquely defined interface and the orientations of their adjacent crystals, this method determines the interface plane normal and thus the interface plane through numerical calculations concerning coordinate system change (based on the Euler angles (φ_1, φ, φ_2) obtained from the above-mentioned EBSD individual orientation measurements) (see Reference [15] for more details). The reticular density was calculated by the position-duplication-number method developed by Fan [21].

4. Conclusions

Sn-Mn alloy was solidified to crystallographically investigate the growth of $MnSn_2$ phase. It was found that:

The non-faced spherical caps of the $MnSn_2$ crystals follow the continuous growth mechanism to grow rapidly along the <001> direction; the side surfaces follow the two-dimensional nucleation mechanism to form the low index {100} and {110} facets.

With an interface structure analysis, it was found that the average reticular density of the atom planes within the {100} IPSP is lower than those within the {011} IPSP so that the {100} planes grow more rapidly than the {110} planes. As a result, the {100} side facets tend to get shorter and then disappear.

Finally, the partially faceted (i.e., non-faceted spherical caps and faceted side surfaces) $MnSn_2$ crystals follow an octagonal-base/spherical-cap geometric model (few crystals possess square bases).

Author Contributions: L.L. wrote the paper; Y.B. performed the experiments; C.B. and H.Z. conceived and designed the experiments; T.L. and X.W. contributed the materials; C.E. and J.C. contributed the data analysis.

Funding: This research was funded by "The [National Natural Science Foundation of China] grant number [51874092, 51690161, 51574073, 51774086 and 51574075]" and "The [National Key Research and Development Program of China] grant number [2016YFB0300901]".

Conflicts of Interest: The authors declare no conflict of interest.

References

1. Corliss, L.M.; Hastings, J.M. Magnetic Structure of $MnSn_2$. *J. Appl. Phys.* **1963**, *34*, 1192. [CrossRef]
2. Kouvel, J.S.; Hartelius, C.C. Abrupt Magnetic Transition in $MnSn_2$. *Phys. Rev.* **1962**, *123*, 124–125. [CrossRef]
3. Kobayashi, T.; Suzuki, K.; Nakamura, N. Optical Recording Medium. U.S. Patent Application No. 4803660, 24 February 1987.
4. Vogt, L.O.; Villevieille, C. $MnSn_2$ negative electrodes for Na-ion batteries: A conversion-based reaction dissected. *J. Mater. Chem. A* **2016**, *4*, 19116–19122. [CrossRef]
5. Mahmoud, A.; Chamas, M.; Jumas, J.C.; Philippe, B.; Dedryv'ere, R.; Gonbeau, D.; Saadoune, I.; Lippens, P.E. Electrochemical performances and mechanisms of $MnSn_2$ as anode material for Li-ion batteries. *J. Power Sources* **2013**, *244*, 246–251. [CrossRef]
6. Philippe, B.; Mahmoud, A.; Ledeuil, J.B.; Sougrati, M.T.; Edström, K.; Dedryvère, R.; Gonbeau, D.; Lippens, P.E. $MnSn_2$ electrodes for Li-ion batteries: Mechanisms at the nano scale and electrode/electrolyte interface. *Electrochim. Acta* **2014**, *123*, 72–83. [CrossRef]
7. Ma, Y.; Gjonnes, J.; Tafto, J. Structure refinement of Al_3Zr using LACBED technique. *Micron Micros. Acta* **1991**, *22*, 163–164. [CrossRef]
8. Li, L.; Zhang, Y.D.; Esling, C.; Jiang, H.X.; Zhao, Z.H.; Zuo, Y.B.; Cui, J.Z. Crystallographic features of the primary Al_3Zr phase in as-cast Al-1.36 wt% Zr alloy. *J. Cryst. Growth* **2011**, *316*, 172–176. [CrossRef]
9. Norby, P.; Christensen, A.N. Preparation and structure of Al_3Ti. *Acta Chem. Scand.* **1986**, *40A*, 157–159. [CrossRef]
10. Li, L.; Zhu, Q.F.; Zhang, H.T.; Zuo, Y.B.; Ban, C.Y.; He, L.Z.; Liu, H.T.; Cui, J.Z. Morphological and crystallographic characterization of solidified Al–3Ti–1B master alloy under a high magnetic field. *Mater. Charact.* **2014**, *95*, 1–11. [CrossRef]
11. Meetsma, A.; Boer, J.L.; Smaalen, S. Refinement of the crystal structure of tetragonal Al_2Cu. *J. Solid State Chem.* **1989**, *83*, 370–372. [CrossRef]
12. Gao, L.; Li, S.M.; Xu, L.; Fu, H.Z. Effect of sample size on intermetallic Al_2Cu microstructure and orientation evolution during directional solidification. *J. Cryst. Growth* **2014**, *394*, 89–96. [CrossRef]
13. Havinga, E.E.; Danmsma, H.; Hokkeling, P. Compounds and pseudo-binary alloys with the $CuAl_2$ (C16)-Type structure. I. Preparation and X-ray results. *J. Less-Common. Met.* **1972**, *27*, 169–186. [CrossRef]
14. Chao, Y.H.; Chen, S.W.; Chang, C.H.; Chen, C.C. Phase Equilibria of Sn-Co-Ni System and Interfacial Reactions in Sn/(Co, Ni) Couples. *Metall. Mater. Trans.* **2008**, *39A*, 477–489. [CrossRef]
15. Zhang, Y.D.; Esling, C.; Zhao, X.; Zuo, L. Indirect two-trace method to determine a faceted low-energy interface between two crystallographically correlated crystals. *J. Appl. Cryst.* **2007**, *40*, 436–440. [CrossRef]
16. Li, L.; Ban, C.Y.; Zhang, R.X.; Zhang, H.T.; Cai, M.H.; Zuo, Y.B.; Zhu, Q.F.; Wang, X.J.; Cui, J.Z. Morphological and crystallographic characterization of primary zinc-rich crystals in ternary Sn-Zn-Bi alloy under a high magnetic field. *Crystals* **2017**, *7*, 204. [CrossRef]
17. Liu, R.P.; Wang, W.K.; Herlach, D.M. Transition from continuous to lateral growth for Ge crystal in undercooled Ge74Ni26 alloy melts. *Scr. Mater.* **1999**, *41*, 855–860. [CrossRef]
18. Mullin, J.W. *Crystallization*, 2nd ed.; LexisNexis Butterworths: London, UK, 1972.
19. Vasudevan, S.; Naoalixgarm, S.; Dwasekaran, R.; Ramasamy, P. Studies on Two-dimensional Nucleation. *Cryst. Res. Technol.* **1981**, *16*, 293–297. [CrossRef]
20. Chadwick, G.A. A Hard-Sphere Model of Crystal Growth. *Met. Sci. J.* **1967**, *1*, 132–139. [CrossRef]
21. Fan, Q.C. A new method of calculating planar density: The position-duplication-number method. *J. Appl. Cryst.* **2016**, *49*, 1454–1458. [CrossRef]
22. Bravais, A.; Etudes, A. *Crystallographiques*; Gauthier Villers: Paris, France, 1866.